6. Strain Gauged IRJ Experiments

6.1. Introduction

To validate the FE model presented in Chapter 4, this thesis has taken advantage of a major field experimental program carried out jointly by the Centre for Railway Engineering (CRE) and Queensland Rail (QR). This experiment involves laboratory tests and field tests. In this chapter, the design of the experiment is presented first in section 6.2. The strain gauge positioning strategy is reported in section 6.3. The manufacturing process of the strain gauged IRJ is introduced in section 6.4. The setup details of lab test and field test are presented in sections 6.5 and 6.6 respectively. Analysis of typical test data is presented in section 6.7 followed by the summary of the chapter in section 6.8.

6.2. Strain-Gauged IRJ Experimental Strategy

The experimental program contained two parts: lab test and field test. The main purpose of the lab test was to ensure the strain gauges were properly working prior to installing in the field. The lab test was conducted in the Heavy Testing Laboratory (HTL) and the field test was carried out in the live railway track. The lab test involved six loading positions as shown in Fig. 6.1 (0mm, 20mm, 50mm, 100mm, 150mm and 200mm from IRJ centre). A static load of 150KN was applied to the railhead and the IRJ was simply supported at the two ends 300mm away from the IRJ centre (end post) as shown in Fig 6.1.

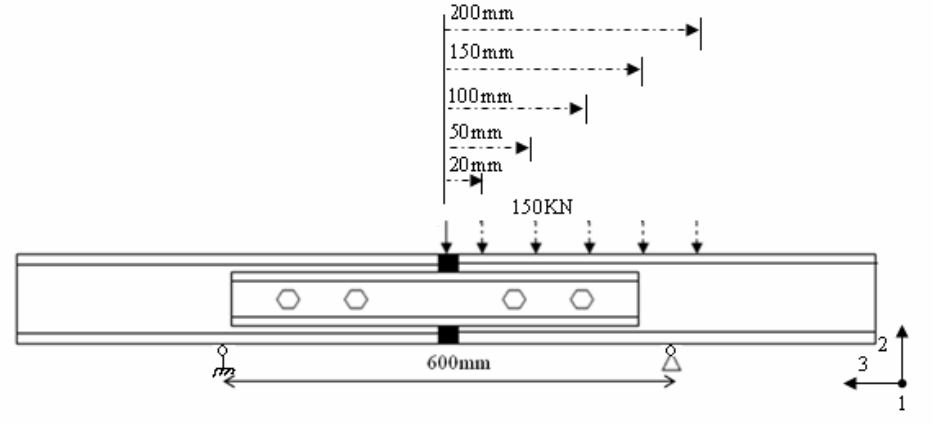

Figure 6.1 Loading positions in lab test

In the field test, the wheel/rail contact impact at the IRJ was indirectly inferred from the strain time series under wheel passages. Referring to Fig. 6.2, the passing wheel triggers the solar powered data recording system using an ultrasonic sensor. The signals from strain gauges were amplified and recorded using the National Instruments DAQ card. The DAQ scanning frequency was set as 20 kHz, sufficient to capture the high frequency dynamic responses. The data recording only occurred for 10 seconds (200,000 data points) with a view to minimising the size of data files. Each passing train triggered collection of the data that were stored in separate files. After each recording, the ultrasonic sensor remained off line for two minutes and started scanning for the next passing wheels.

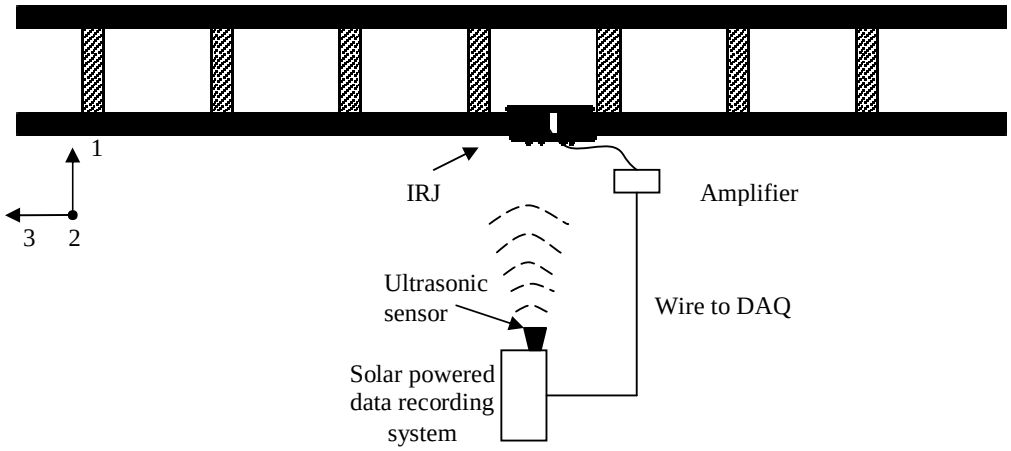

Figure 6.2 Data recording system for the field test

6.3. Strain Gauge Positioning Strategy

Positioning of the strain gauges is critical to the successful outcome of this experiment. As a principle, the locations for strain gauges should be fairly sensitive to the high magnitude strains under static and dynamic loads whilst being technically feasible. To acquire the IRJ impact response that is of interest, the strain gauges are also required to be as close as possible to the end post and railhead. Strain gauges can only be placed on the surfaces of IRJ parts; the top of the railhead surface is automatically excluded because of the wheel passage; the rail ends are also excluded as it would be difficult to detail the strain gauge wires and strain gauges in a safe manner. As a result, the rail web, the rail bottom and the joint bars are possible locations. Numerical results from the dynamic FE model are employed to identify the most sensitive positions for locating the strain gauges.

Determining the rail strain is a complex problem. This is because rail is constantly subjected to thermal strain and under the action of wheel loads; it is subjected to bending and shear stresses. Therefore three surface strains (two normal and one shear) on two mutually perpendicular planes would establish six independent strain components. As two of the out of plane shear strains (E_{12} & E_{13}) and lateral normal strain E_{11} are of less significance in tangent track rails (without regard to braking/traction forces), only three strain components that are sensitive to the wheel/rail normal contact (the vertical normal strain E_{22}, the shear strain E_{23} and longitudinal normal strain E_{33}) have been measured. The FE results indicate that the rail web is sensitive to the E_{22} and the E_{23} while the rail bottom is more sensitive to the E_{33}. The joint bars are not sensitive to any of the important strain components.

The snap shots of the vertical strain distribution from the dynamic analysis corresponding to three wheel positions (15mm before end post, at end post and 15mm after end post) are shown in Fig. 6.3 (a), (b) and (c) respectively. Before the wheel hitting the end post, the maximum strain value is shown as $430\,\mu s$ located at the fillet radii between the railhead and the web, 110mm above rail bottom. For the wheel loading at 0mm and 15mm after the end post, the maximum strains are $660\,\mu s$ and $620\,\mu s$ respectively. These strain values are sufficiently large for reasonable measurement accuracy by electrical strain gauges.

Hence, there are four symmetric points (1, 2, 3&4) on both sides of rail web at both rails selected for gauging the vertical normal strain E_{22} and shear strain E_{23} shown in Fig. 6.4. The longitudinal normal strain on the rail web, although captured by these strain gauge rosettes, remain very small throughout the wheel travel in the vicinity of the end post.

For the longitudinal strain E_{33}, the most sensitive and practical position is the rail bottom. Referring to Fig. 6.5, with the wheel load at the IRJ centre, the maximum longitudinal bending strain is around $64.2\,\mu s$. The contour demonstrates a symmetric distribution of E_{33} at the bottom of both rail ends. E_{33} is concentrated at the positions approximately 60mm away from the joint. Hence the strain gauges (Strain gauge 5 & 6) are symmetrically positioned to measure the E_{33} as shown in Fig. 6.6.

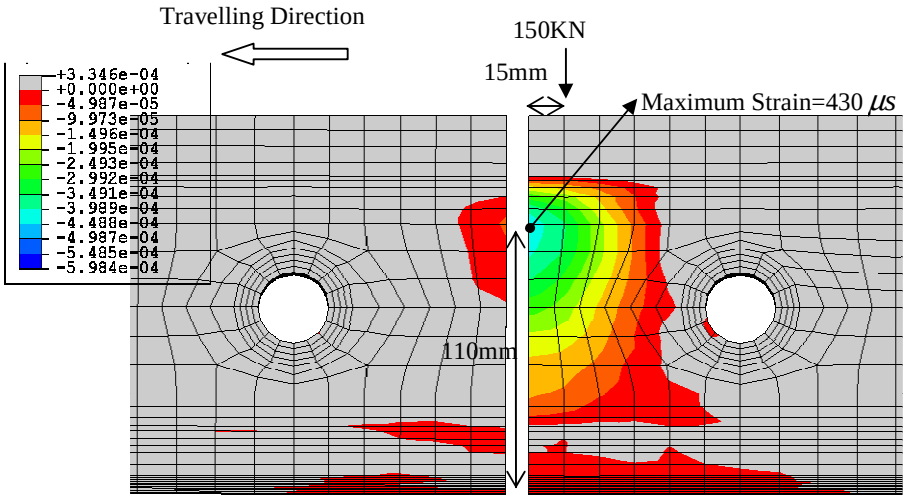

(a) Pre impact

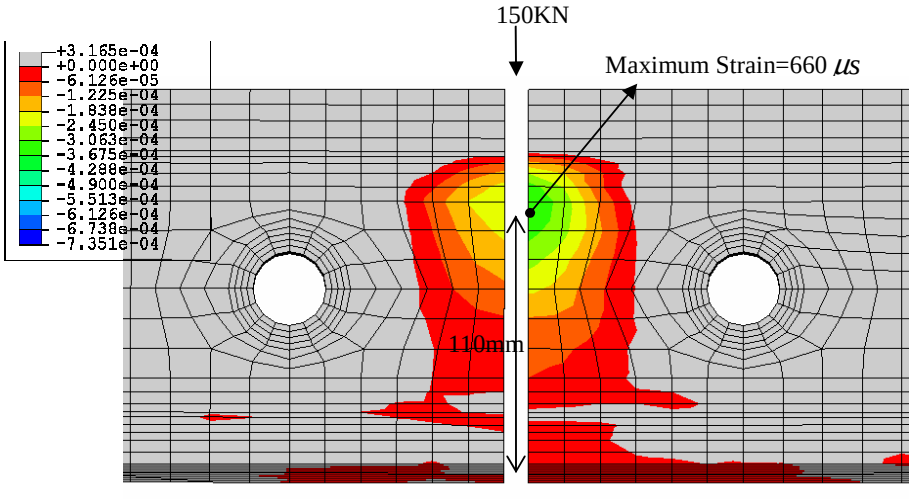

(b) At impact

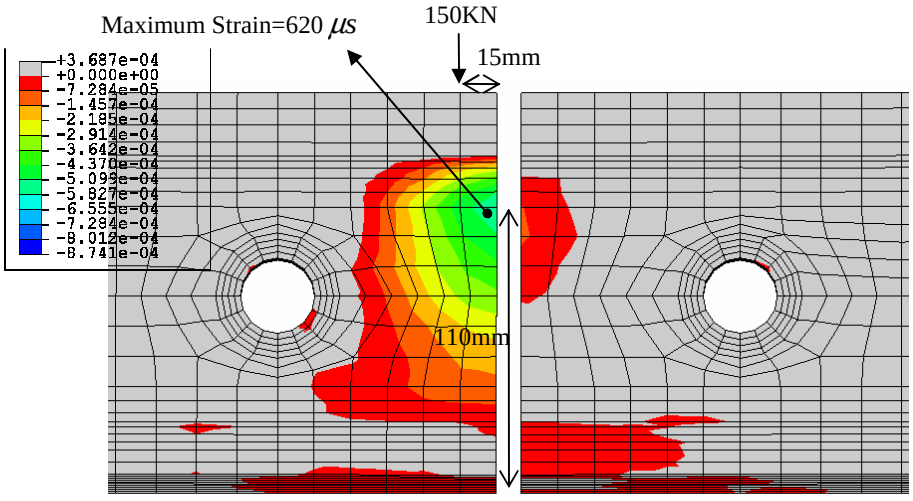

(c) Post impact

Figure 6.3 Snap shots of the vertical strain distribution from the dynamic analysis

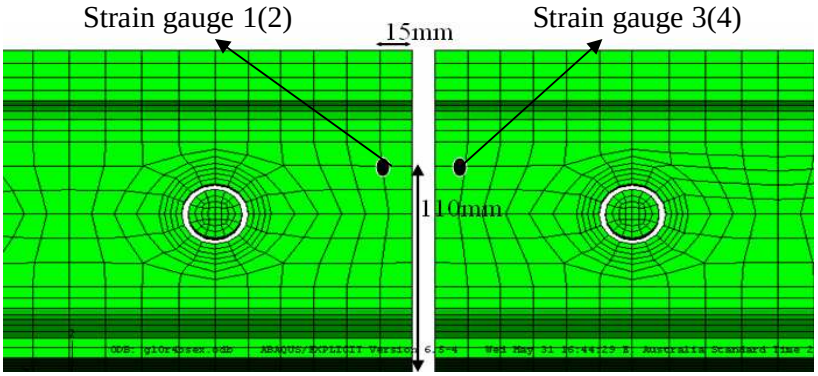

(a) Longitudinal view

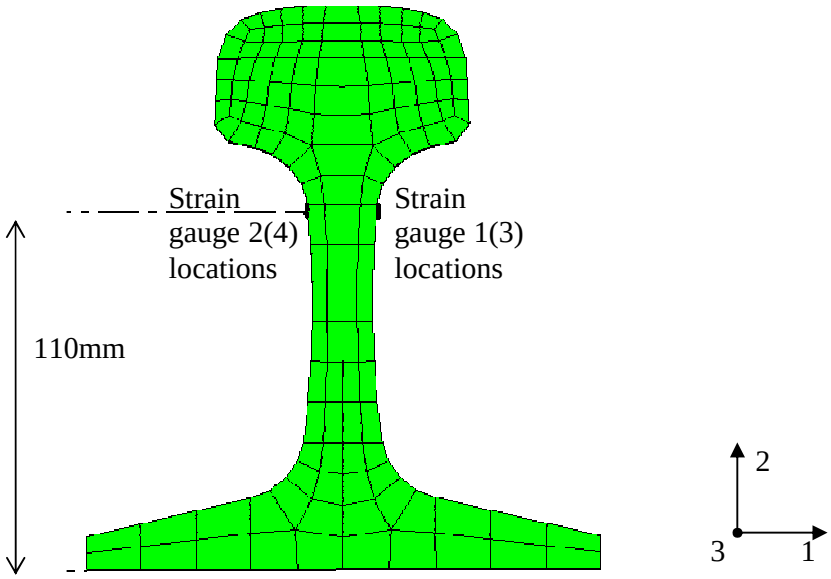

(b) End view

Figure 6.4 Strain gauge positions for E_{22} and E_{23} measurements

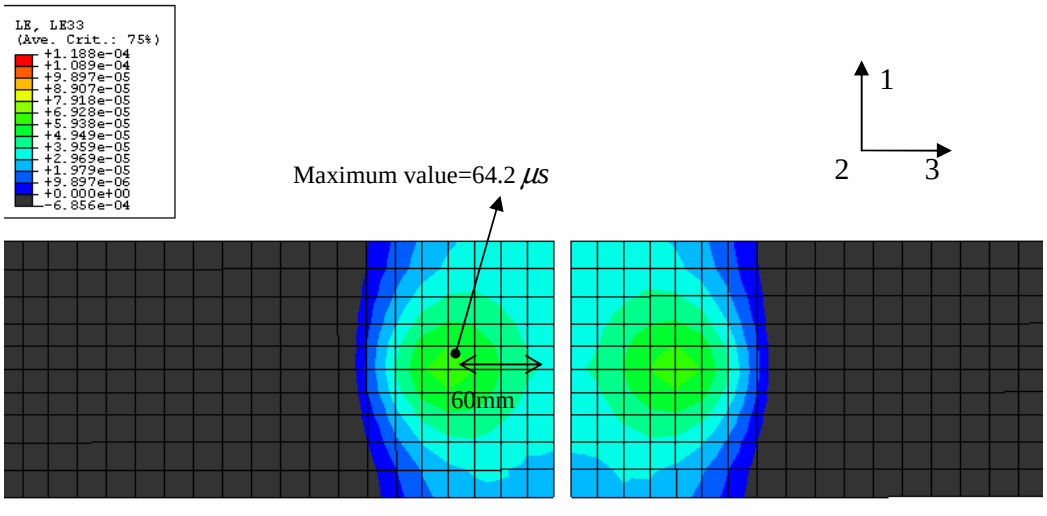

Figure 6.5 E_{33} distribution on the rail bottom

In summary, there are six positions on two both rail sections (four on rail web and two on rail bottom) of IRJ selected for strain gauging. Strain gauges 1, 2, 3 and 4 on the rail web surface are used for E_{22} and E_{23} measurement and Strain Gauges 5 and 6 on the bottom are selected to measure the E_{33}.

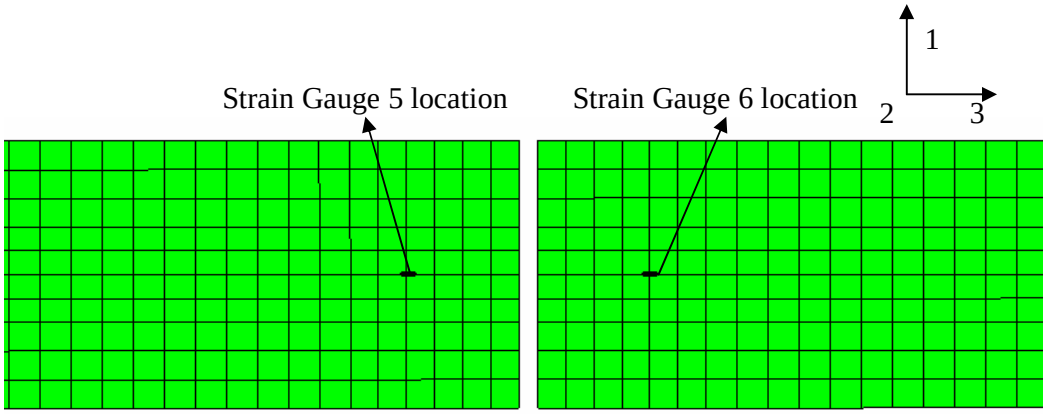

(a) Bottom view

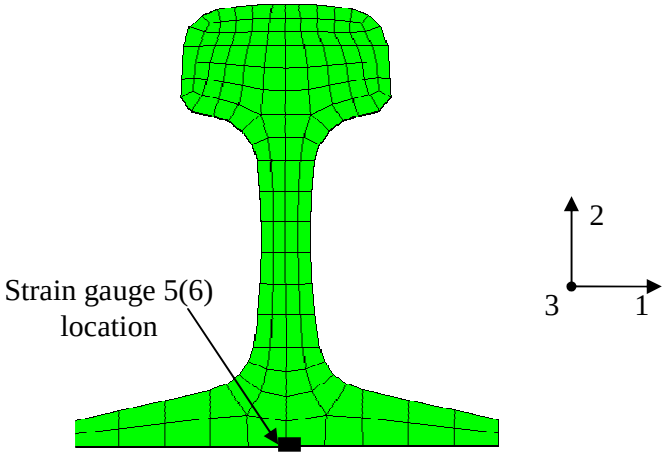

(b) End view

Figure 6.6 Strain gauge positions for E_{33} measurements

6.4. Preparation of Strain Gauged IRJ

6.4.1. Selection of strain gauge rosette

The 45˚ 3-gauge rosette selected for the measurement of the vertical normal strain E_{22} and shear strain E_{23} is shown in Fig. 6.7. The middle gauge B is aligned in

the vertical direction for the E_{22} measurement, and the E_{23} is calculated from the two 45˚ aligned gauges A and C. A linear gauge D is used at the rail bottom surface for the E_{33} measurement. Eq. (6.1) was used to convert the measured linear strains to the normal and shear strain:

$$\begin{aligned} E_{22} &= E_{BB} \\ E_{23} &= E_{CC} - E_{AA} \\ E_{33} &= E_{DD} \end{aligned} \tag{6.1}$$

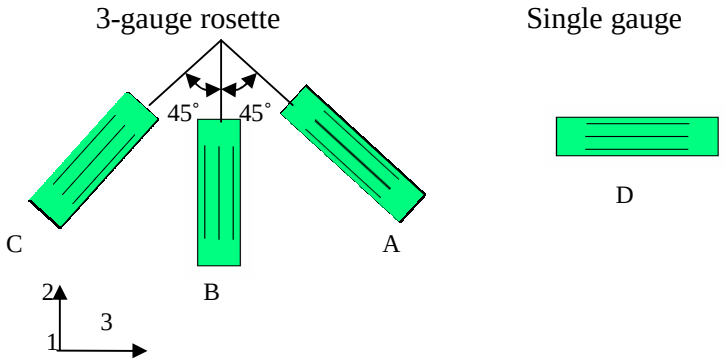

Figure 6.7 Strain gauge rosettes

To withstand the high temperature involved in the IRJ assembling process, Vishay Micro-Measurement CEA gauges with a fully encapsulated grid and exposed copper-coated integral solder tabs were selected. This strain gauge had a wider working temperature range from (-50˚C) to (+250˚C).

6.4.2. Installation of strain gauges on IRJ

The strain gauges were positioned at the rail web and the rail bottom. Installation of the rail web strain gauges was comparatively more complex as they were positioned on the rail web covered by the joint bar. The rail bottom strain gauges were stuck on the exposed rail bottom surface after the IRJ was fabricated in the factory.

The rail web strain gauges were installed during the process of assembling of the IRJ in the factory. First the strain gauges were stuck on both sides of the rails (Fig 6.8). The rail bottom strain gauges were stuck on after the IRJ was assembled in the factory, and covered with a plastic layer of water proofing material.

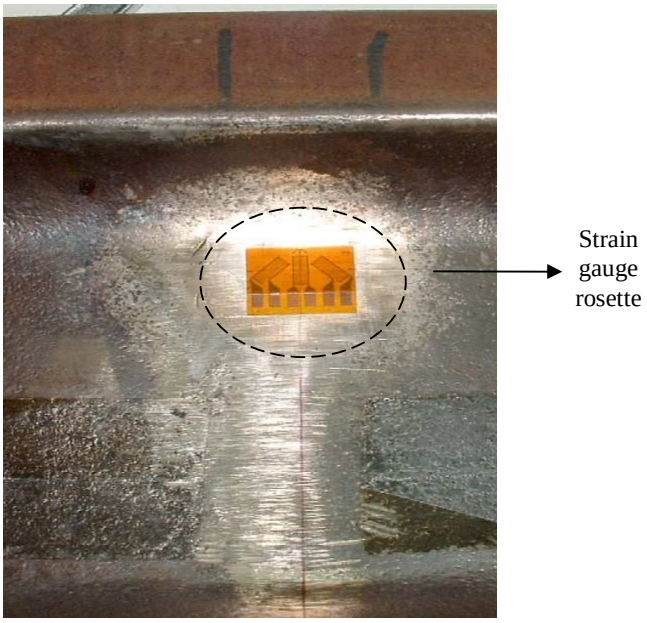

Fig 6.8 Strain gauges stuck to the rails

6.5. Lab Test of Strain Gauged IRJ

In this section, details of IRJ laboratory test setup are presented. Some typical test data are also reported; the data were used to validate the FE model as described in the next chapter.

6.5.1. Laboratory test setup

The overall IRJ test setup in the laboratory is displayed in Fig. 6.9. The IRJ was supported on two steel bars in such a way that the rail bottom surface contacted with

the bar top surface. The smooth contact surfaces between the rail bottom and the steel bars allowed the IRJ to move freely in the longitudinal direction. The span of the IRJ was kept as 600mm. The static load driven by the actuator was transferred to the railhead through a steel block. The steel block was provided with the railhead profile to ensure a conforming contact. The actuator was driven by a hydraulic pump and the loading rate was controlled as 1kN/s to satisfy the static loading hypothesis. Fig 6.10 shows how the load was transferred from the actuator to the railhead.

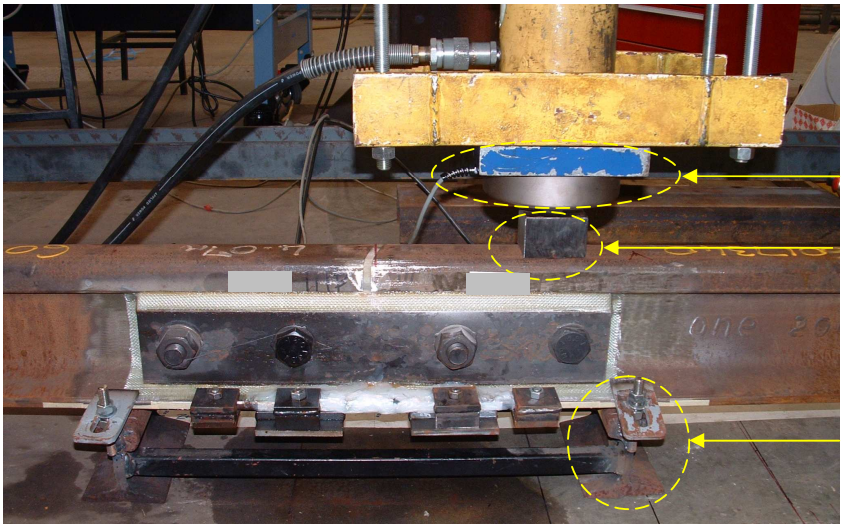

Figure 6.9 Lab test setup

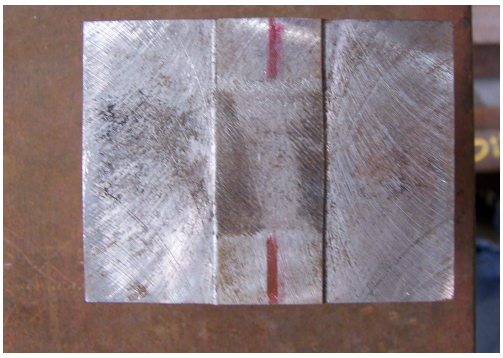

(a) Loading block

(b) Load transfer to railhead

Fig 6.10 Loading equipments

The strain gauge response signal was acquired by four 4-channel National Instruments DAQ cards. In this lab test, all fourteen strain gauge channels were connected to the

DAQ card for data collection. The Quarter-Bridge type was employed for the strain gauge circuit (Fig 6.11), where the $R1 = R2 = 500\Omega, R3 = 350\Omega$ are resistors, $Rl = 2.76\Omega$ is the wire resistance and strain gauge resistance $Rg = 350\Omega$. $Vex = 5V$ is the bridge excitation voltage and Vo is the calibrated bridge output voltage. The strain is calculated from the voltage as:

$$\varepsilon = -4Vr * (1 + Rl / Rg) / [GF * (1 + 2Vr)] \tag{6.2}$$

Where $Vr = (Vo / Vex)$ and gauge factor GF is 2.11 in this case.

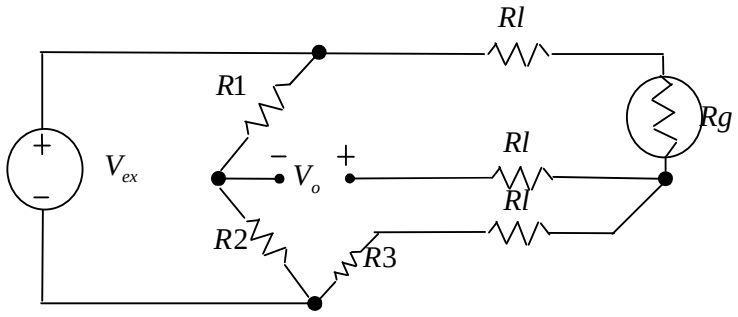

Fig 6.11 Quarter-bridge routine for strain gauges

6.5.2. Typical data

The data collected from the strain gauges were converted to the objective strain components: vertical normal strain E_{22}, shear strain E_{23} and longitudinal strain E_{33} using Eqs. (6.1) and (6.2). Strain gauges 1, 2, 3 and 4 were used for E_{22} and E_{23} measurement and strain gauges 5 and 6 on the rail bottom were used for E_{33}.

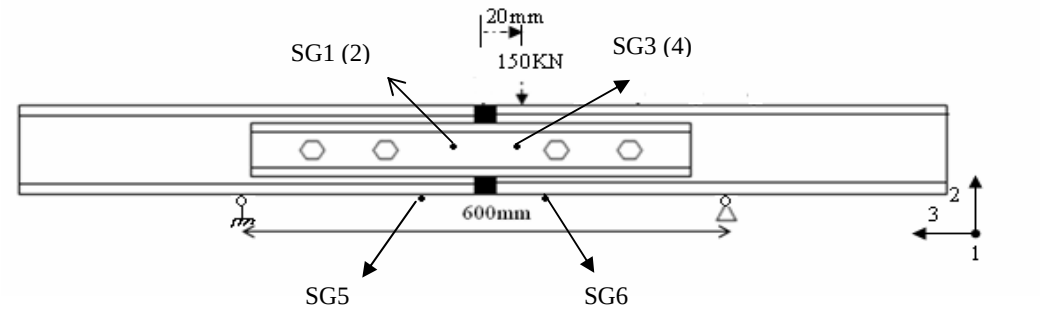

Fig 6.12 Illustration for position of strain gauges and load

It was extremely difficult to ensure the symmetry of loading (see Fig. 6.10); some eccentricity was unavoidable. Therefore it was found that the strain data collected from Strain Gauges 1 and 2 and Strain Gauges 3 and 4 varied. To ensure linearity and repeatability checks, it was considered sufficient to average the corresponding strains to both sides of the rail web. Fig. 6.12 shows that the loading position is 20mm away from the IRJ end post centre. Fig. 6.13 and 6.14 indicate that under the 150KN static load, E_{22} from Strain Gauges 1/2 is 35.6 microstrain and 464.7 μs for Strain Gauges 3/4. The shear strain E_{23} for the Strain Gauge 1/2 is 47.1 μs while Gauges 3/4 show a value of 234.5 μs. The longitudinal tensile strain is plotted in Fig. 6.15. It indicates that Strain Gauges 5 and 6 have had a very similar magnitude of 118.2 μs and 123.1 μs respectively.

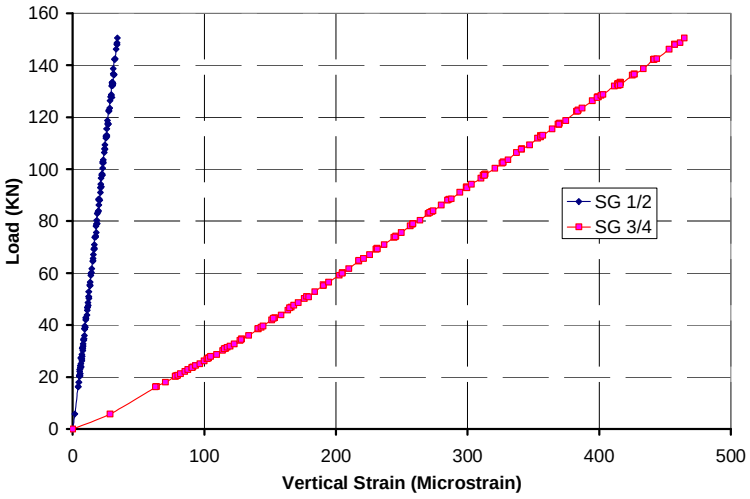

Figure 6.13 Averaged vertical strain E_{22}

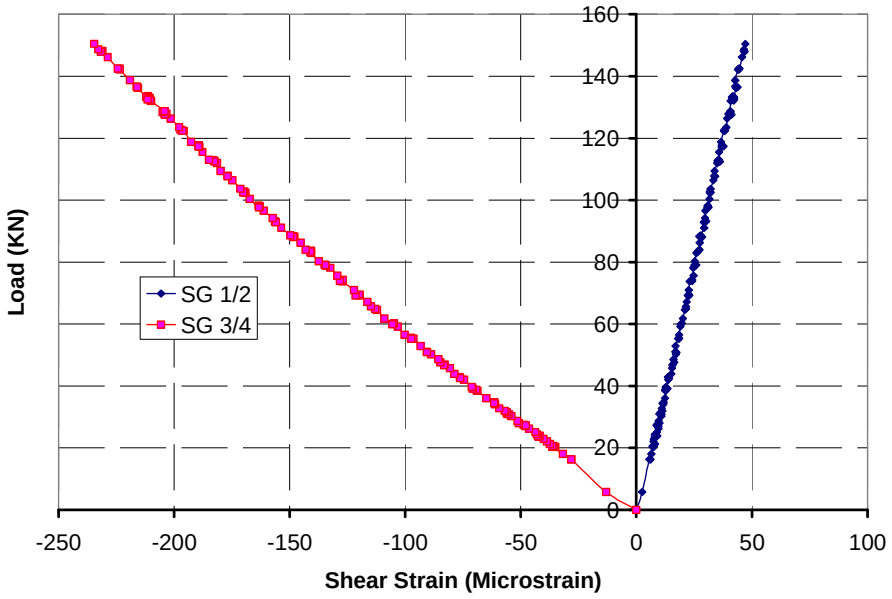

Figure 6.14 Averaged shear strain E_{23}

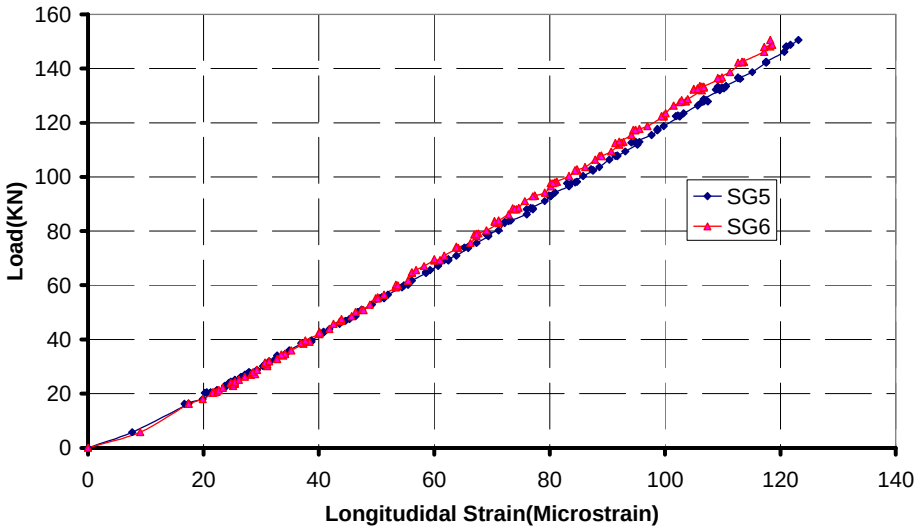

Fig 6.15 Longitudinal strain E_{33}

6.6. Field Test of the Strain Gauged IRJ

In this section, the details of IRJ field test setup are presented and the typical test data are also reported.

6.6.1. Field installation

The strain gauged IRJ was installed in the field by replacing a continuous weld rail section (Fig. 6.16). A data recording housing was built near the track for automatic wheel passage detection and data recording.

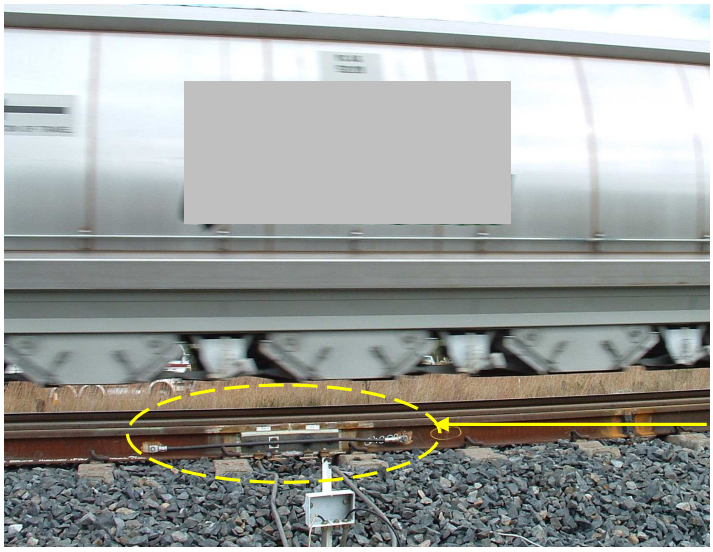

Figure 6.16 Installed strain gauged IRJ as a wagon is passing over

The wires from strain gauges were connected to an amplifier used to amplify the voltage signals to improve the signal reception. The signals from the amplifier were transferred to the data recording system. A solar powered data recording system consisted of a National Instruments compact DAQ and Logger, ultrasonic sensor, solar panels (2 x 80W), charger and storage hard disk.

The strain gauge circuit used in the field test was the same as that of the lab test. Due to the limited number of DAQ channels, the strain gauges on only one rail of the strain gauged (Strain gauge 1, 2 and 5) IRJ were activated. The DAQ channel scanning frequency was kept as 20 kHz and the recording duration for each passing train was limited to 10s, which corresponded to 200,000 data points from each channel for each train. A data processing programming was coded in MATLAB.

6.6.2. Typical data

In this field test, Strain gauges 1 and 2 were used for monitoring E_{22} and E_{23} and Strain gauge 5 was used for measurement of E_{33} . The converted strain components E_{22} , E_{23} and E_{33} are presented in Fig. 6.17, Fig 6.18 and Fig. 6.19 respectively.

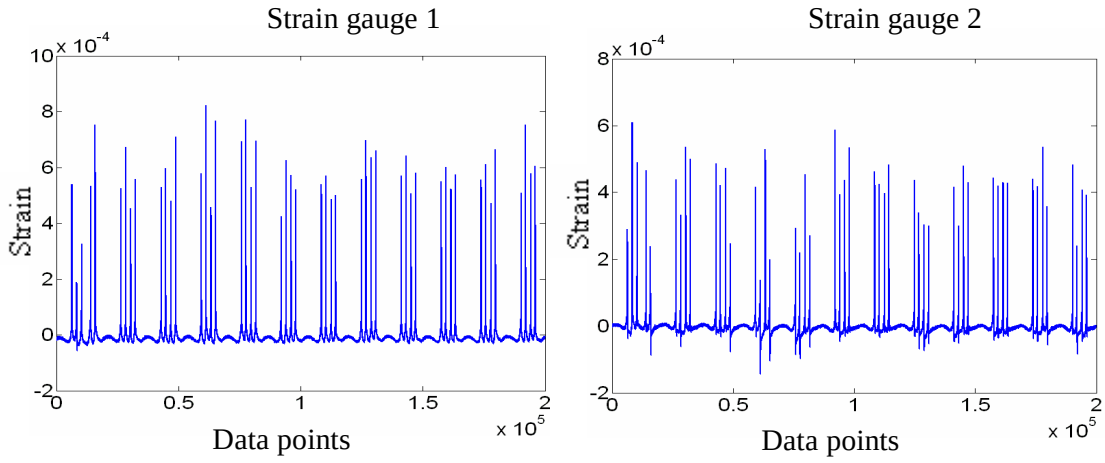

Figure 6.17 Vertical normal strain E_{22} history

It can be seen there are many ‘impacts’ in each file and each ‘impact’ represents a passing wheel. The horizontal axis is the recorded data point number (which can be converted to time divided by 20,000) and the vertical axis is the strain magnitude. The

recorded peak value of E_{22} and E_{23} are in the order of 10^2 μs while E_{33} has a lower value at the order of 10^1 μs. The strain time series of E_{33} exhibits quite noisy signals due perhaps to the strain gauges being located away from impact locations. Furthermore, longitudinal strains are affected by flexure due to other wheels as well as thermal longing.

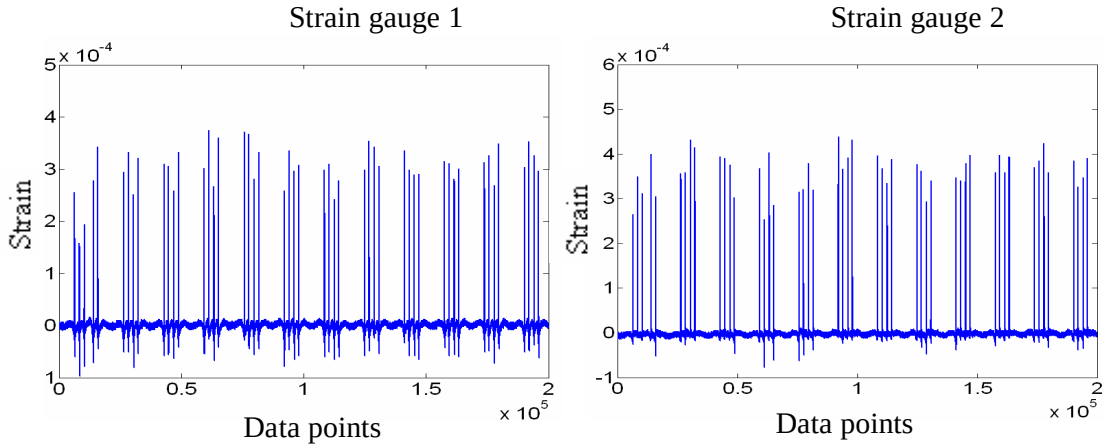

Figure 6.18 Shear strain E_{23} history

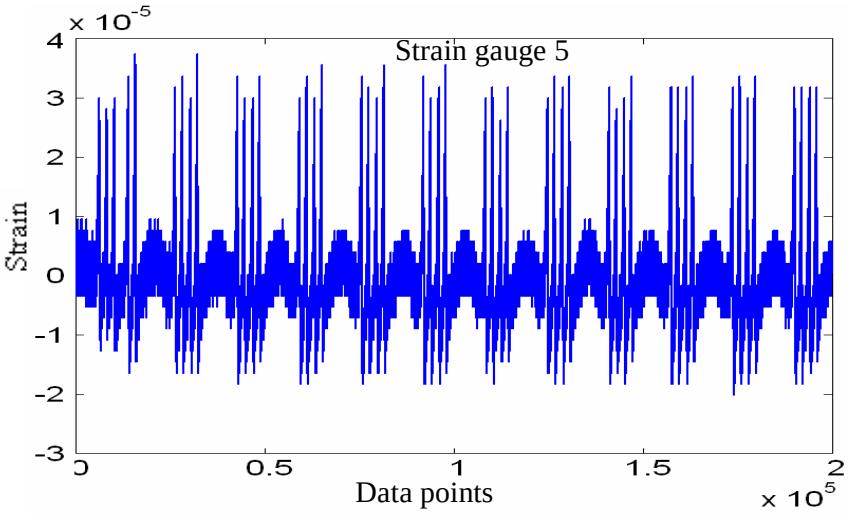

Figure 6.19 Longitudinal strain E_{33} history

The data from Strain gauge 1 are shown in Fig. 6.19; this indicates that the strains on both sides of the rail caused by the passing wheels are different due primarily to

eccentric positioning of the wheels. As an approximation in the first stage of analysis, the eccentricity in the wheel position was disregarded as the strain data from Strain gauges 1 and 2 were averaged. Figs. 6.20 and 6.21 present the averaged strain components E_{22} and E_{23}. A set of even peaks are shown in these figures because the wheel eccentricity was eliminated.

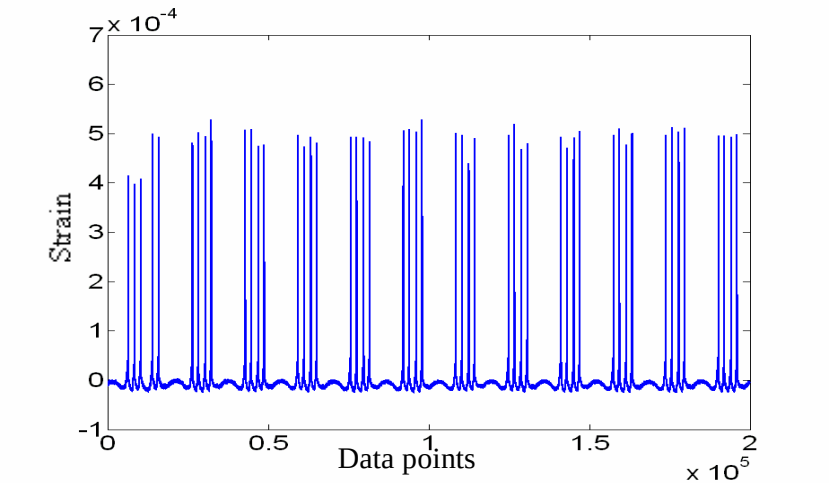

Figure 6.20 Averaged vertical normal strain E_{22} history

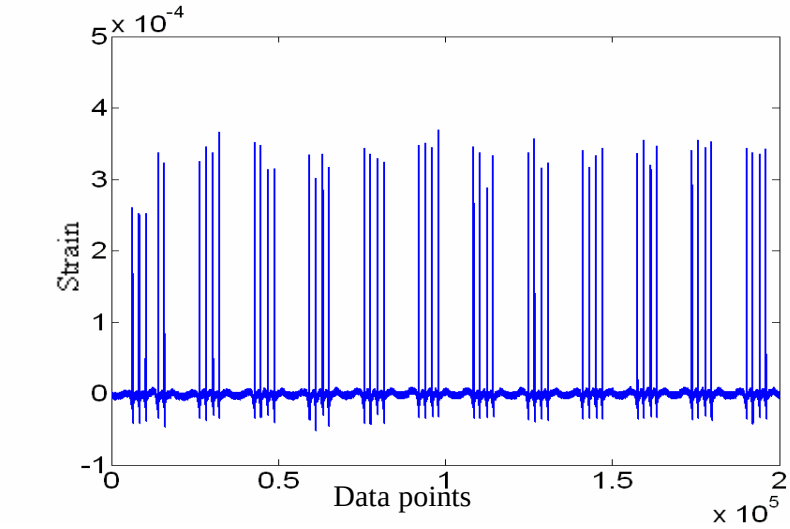

Figure 6.21 Averaged shear strain E_{23} history

6.7. Analysis of Field Data

The field traffic condition is an important factor for FE model validation. A close examination of the field test data helps with understanding the traffic condition and the characteristics of the wheel/IRJ impact as described in this section.

6.7.1. Traffic classification

As the IRJ was subjected to mixed traffic conditions with coal, freight, and passenger trains travelling at different speeds, different axle loads and even different directions, it became necessary to sort out the data according to the type of train prior to analysing the strain history carefully.

Fig. 6.22 illustrates the averaged vertical normal strain data E_{22} corresponding to an unknown train. All we can state is that each impact represents a passing wheel. As the data show that there are 5-impacts as a 'group' (shown circled in Fig. 6.22) at the beginning of the record, it is inferred that the five impacts correspond to that of the rear bogie (three axles) of a diesel locomotive and the front bogie (two axles) of a wagon. It should be noted that due to the delay in triggering of the DAQ system by the ultrasonic sensor, generally the first three bogies of the two locomotives are missed. Subsequent impacts occurred generally in groups of four wheelsets.

The traffic condition is worked out by conducting the data analysis with additional help of QR operational data. Due to confidentiality, the processing details of traffic conditions are not provided in this thesis. The sorted out traffic condition was applied to the FE model for model validation.

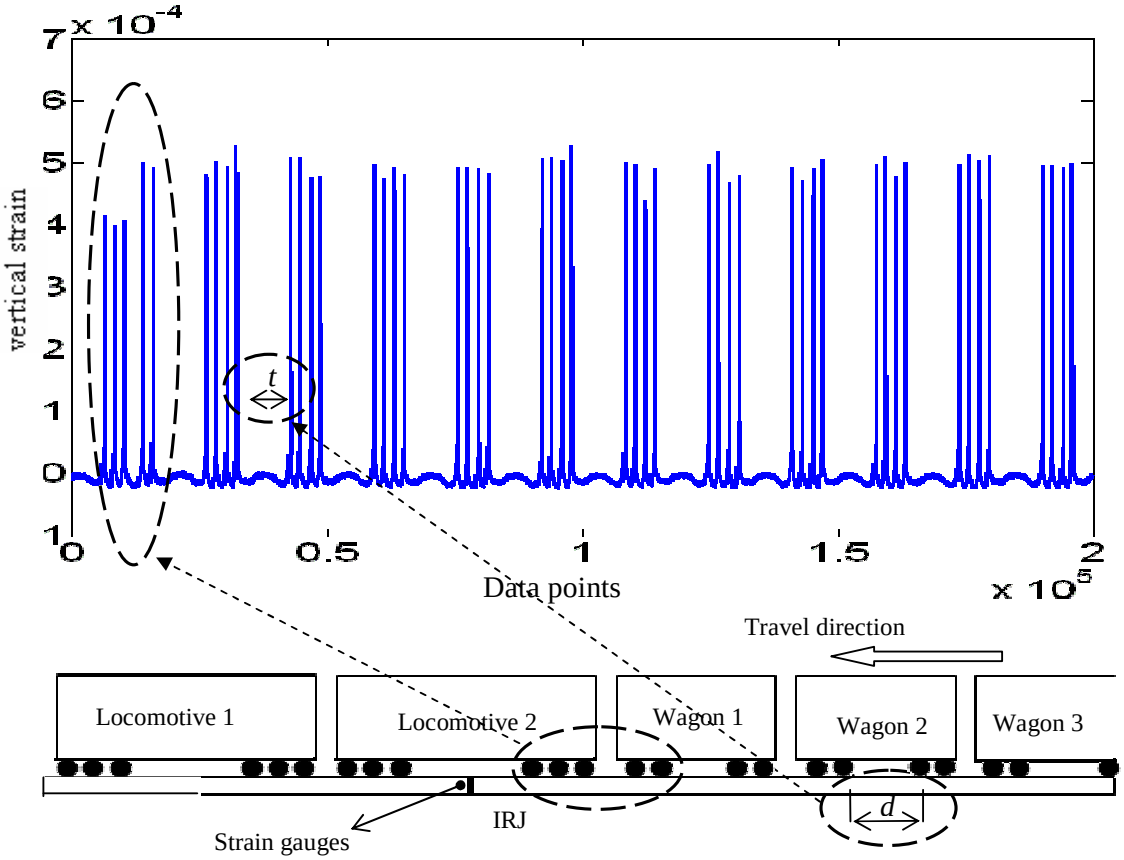

Figure 6.22 Illustration of rollingstock travelling in field test

6.7.2. Vertical strain signature

By zooming into one of the 'impacts', the strain signature caused by the moving wheel load is examined. Typically two types of strain signature were found according to different travelling directions. The first signature is shown in Fig. 6.23 where the strain remains at near zero magnitude before the wheel hits the IRJ. As the wheel approaches the IRJ, the strain value sharply increases to a peak value of 491.9 μs within a very short duration. After impact, the strain value damped relatively slowly. It is notable that the passing wheel causes two peaks when the strain gauge is located after the joint. The first peak has a higher magnitude than the second peak. The time interval between the two peaks is 0.95 ms corresponding to approximately

20.0mm with the train longitudinal velocity of 74.5Km/h. Considering the strain gauge located 15 mm from rail end and the thickness of end post material being 10mm, it is believed that the first peak is generated by the wheel/IRJ impact and the second peak is due to the wheel passing above the strain gauge position (15mm from the rail end) as shown in Fig 6.26. It indicates that the wheel/rail impact at the IRJ is captured in this signature.

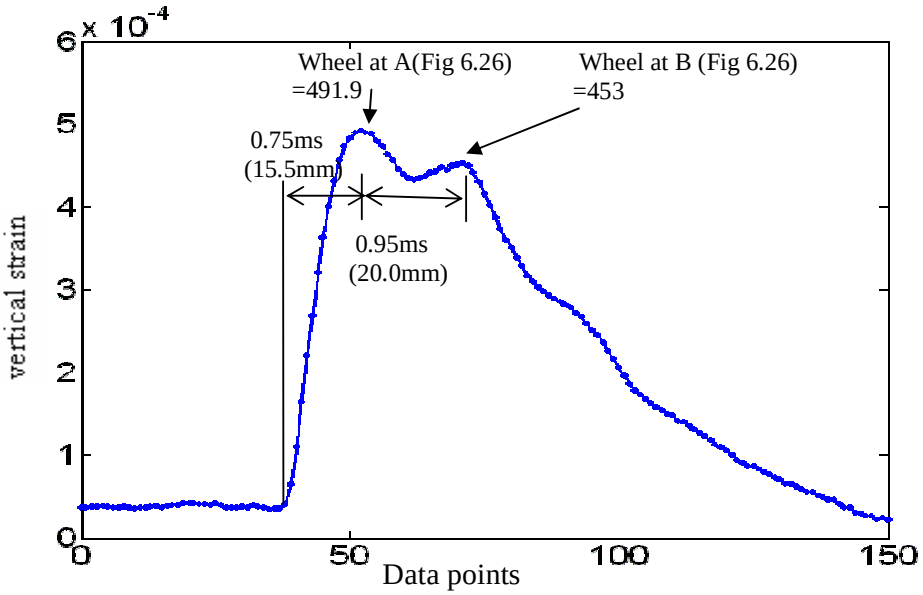

Figure 6.23 Zoom-in of vertical strain history for a wheel passage

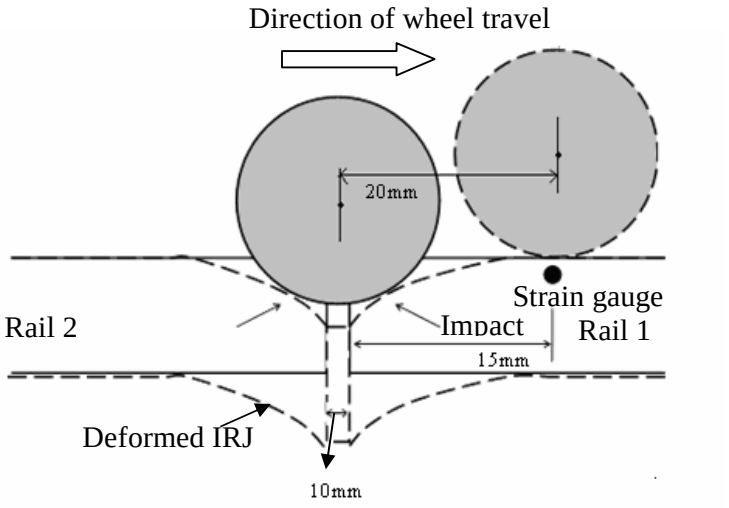

Figure 6.24 Illustration of two peaks generating mechanism

The second signature records a train travels in the opposite direction to the above case. The signature changes as shown in Fig. 6.25. In this case, the strain increases gradually to a peak value. After reaching the peak value it dives sharply to a constant level near zero. As the 'two peak' form does not appear, it is inferred that the impact is not acquired by the strain gauges as they are positioned on the 'first' rail end, referring to Fig. 6.26. It is also inferred that, although the impact is generated by 'two-point contact', the impact force is mostly concentrated on the 'second' rail end of the IRJ.

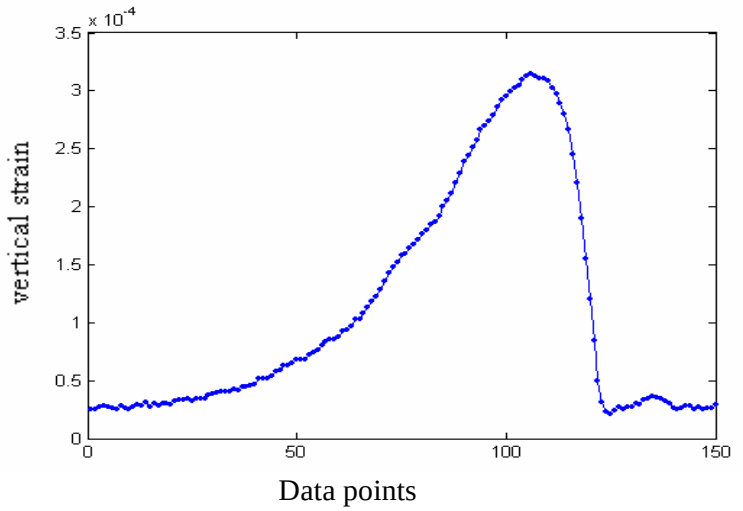

Figure 6.25 Zoom-in of vertical strain history for a wheel passage transporting in an opposite direction

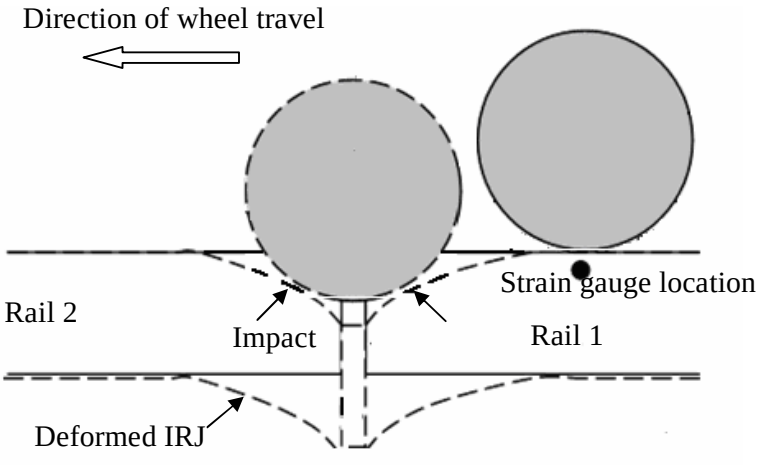

Figure 6.26 Illustration of one peak generating mechanism

6.8. Summary

The strain gauged experiment introduced in this chapter provides a platform to validate the FE model of wheel/rail contact-impact at the IRJ. The static loading experiment was carried out prior to the major field test. The field test was carried out in the live railway track that was designed to capture the dynamic response of the wheel/rail contact impact. The dynamic FE model was employed to identify the best possible locations for strain gauges.

In the lab test it was difficult to ensure the exact symmetry of the application of loading. In the field wheels generally run unsymmetrically on the rail head. As such, both tests have exhibited varying levels of strains on opposite faces of the rails due to lateral bending caused by eccentric loading. The strains were therefore averaged and all analyses thus considered a pseudo symmetric loading state. From the field strain data, it was shown that the traffic direction could be identified. It was also possible to sort out the data as per the type of wagons. The data are used to validate the FE models (static and dynamic) as reported in Chapter 7.